

Precise timing of abrupt increase in dust activity in the Middle East coincident with 4.2 ka social change

Stacy A Carolin¹, Richard Walker¹, Christopher Day¹, Vasile Ersek², R Sloan³, Michael Dee⁴, Morteza Talebian⁵, Gideon Henderson¹

¹University of Oxford, ²Northumbria University, ³University of Cape Town, ⁴University of Groningen, ⁵Geological Survey of Iran, Azadi Square, Meraj Blvd, Tehran, Iran

Submitted to Proceedings of the National Academy of Sciences of the United States of America

The extent to which climate change causes significant societal disruption remains controversial. An important example is the decline of the Akkadian Empire in northern Mesopotamia ≈ 4.2 ka, for which the existence of a coincident climate event is still uncertain. Here we present an Iranian stalagmite record spanning 5.2–3.7 ka, dated with 25 U/Th ages that provide an average age uncertainty of 31 years (1σ). We find two periods of increased Mg/Ca, beginning abruptly at 4.51 and 4.26 ka, and lasting 110 and 290 years, respectively. Each of these periods coincides with slower vertical stalagmite growth and a gradual increase in stable oxygen isotope ratios. The periods of high Mg/Ca are explained by periods of increased dust flux sourced from the Mesopotamia region, and the abrupt onset of this dustiness indicates threshold behavior in response to aridity. This interpretation is consistent with existing marine and terrestrial records from the broad region, which also suggest that the later, longer event beginning at 4.26 ka is of greater regional extent and/or amplitude. The chronological precision and high resolution of our new record indicates that there is no significant difference, at decadal level, between the start date of the second, larger dust event and the timing of North Mesopotamia settlement abandonment, and furthermore reveals striking similarity between the total duration of the second dust event and settlement abandonment. The Iranian record demonstrates this region's threshold behavior in dust production, and ability to maintain this climate state for multiple centuries naturally.

4.2 ka event | stalagmite | drought | Mesopotamia | dust

Main Body Text:

The characteristics of an anomalous, abrupt climate event at ≈ 4.2 ka (thousand years before 1950 C.E.) remain controversial. Multiple advanced societies, including the Akkadian Empire, Ancient Egypt, and Indus Valley civilizations, experienced great transformations at ≈ 4.2 ka (e.g. 1). A climate event is seen in other paleoclimate records at about this time (2–11), leading some to hypothesize a possible cause-and-effect relationship between climate change and societal change (12,13). There is, however, no *a priori* reason to expect a climate anomaly at 4.2 ka, as it post-dates the deglaciation and is a time when potential climate drivers (CO_2 (14), volcanic emissions (15), solar output (16), etc.) have levels similar to modern and do not show an abrupt or significant change. It is possible that the 4.2 ka event was a result of stochastic atmospheric forcing, and might be part of a pattern of decadal/centennial climate variability in this region more generally. Resolving the nature of Middle-Eastern climate change during this period, and particularly the timing and duration of the event at ≈ 4.2 ka, is important to understand the natural climate variability of this region, critical for both historical and modern human society.

The most prominent evidence for an abrupt, anomalous climate event in the Middle East region at ≈ 4.2 ka is found in two marine records. The first is a multi-proxy sediment record from the northern Red Sea (Fig. 1, Label 1) that suggests an abrupt dry event beginning at $4.2 \pm 0.1(1\sigma)$ ka (Fig. 2a) (5). The second is a

sediment core record from the Gulf of Oman (Fig. 1, Label 2) that shows an abrupt increase in Mesopotamia-sourced dust deposition at $4.1 \pm 0.1(1\sigma)$ ka (Fig. 2a) (3). These events occur within error of each other, and within error of the precisely dated end of the Akkadian empire in northern Mesopotamia, $4.19 \pm 0.02(1\sigma)$ ka (17). The level of this correlation is uncertain, however, because the start date and duration of the climate events found in existing sediment records is limited to centennial precision by the low sampling resolution and age errors intrinsic to ^{14}C -dated marine records (SI Appendix, Fig. S1). In addition, inter-annual rainfall variability over the northern Red Sea is not strongly correlated in modern times with rainfall variability at Tell Leilan (Fig. 1, Label '+'), the archeological site that originally and most-convincingly establishes the timing of the abrupt abandonment of urban settlements and decline of the Akkadian empire in northern Mesopotamia (12, 17).

The presence of a regional, or even global-scale, multi-century climatic event beginning at ≈ 4.2 ka has been suggested by multiple other studies (e.g. 2,4,6–11) both within and beyond the Middle East region. Of these, speleothem records have the potential to provide particularly precise age control to improve on chronologies of marine records. None of the speleothem records from the eastern Mediterranean and West Asia region, where inter-annual rainfall variability under modern conditions is correlated to the rainfall variability of northern Mesopotamia, however, show an abrupt, anomalous $\delta^{18}\text{O}$ signal comparable to that observed in the two marine records at ≈ 4.2 ka (Fig. 2a). Lack

Significance

A speleothem geochemical record from northern Iran captures significant climate fluctuations during the mid-to-late Holocene at high resolution. Two abrupt shifts in Mg/Ca last for more than a century and are interpreted as enhanced dust activity, indicating a threshold behavior in response to aridity. Coincident gradual peaks in $\delta^{18}\text{O}$ support the interpretation of regional drying. The precise chronology shows the later event, 4.26 to 3.97 ka, is coincident within decades of the period of abandonment of advanced urban settlements in northern Mesopotamia, strengthening the argument for association between societal and climatic change. The record demonstrates the abrupt onset of dust production in the region, and ability to maintain this dry climate state for multiple centuries naturally.

Reserved for Publication Footnotes

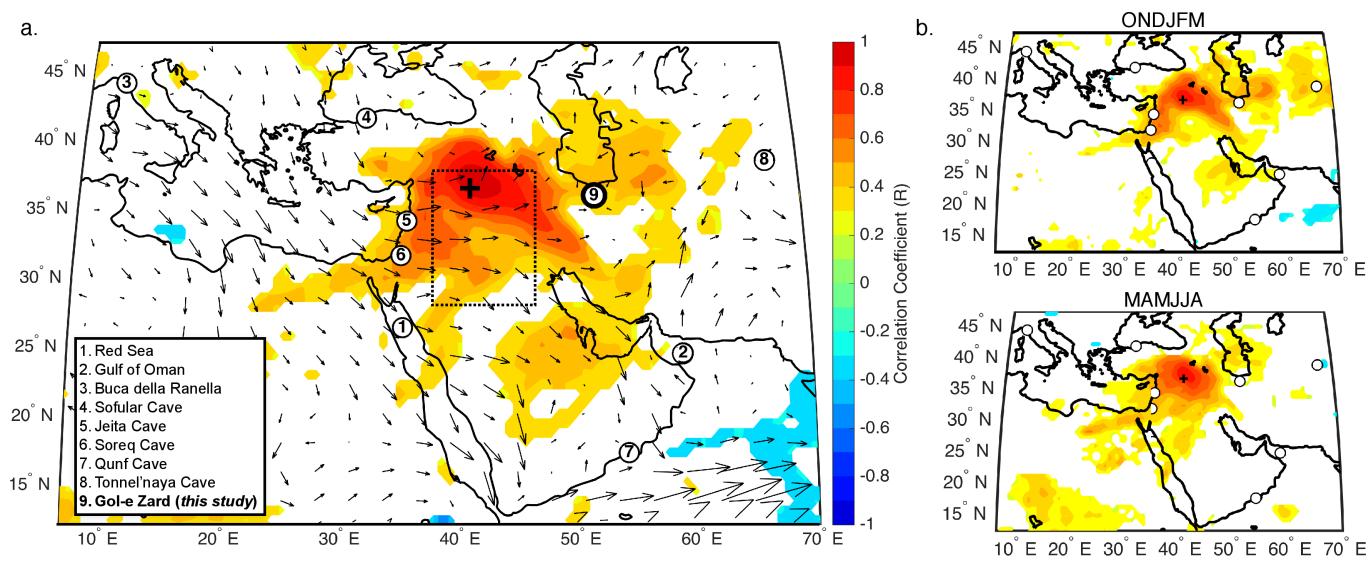


Fig. 1. . Correlation maps of archeological site Tell Leilan (black '+') rainfall with ECMWF ERA-Interim model forecast total precipitation (resolution ≈ 80 km) (41). White areas indicate areas where $p > 0.10$. The Tell Leilan rainfall record was set as the ERA-Interim model forecast record at the closest point (37°N , 41.5°E). Annual precipitation records in (a) were constructed by calculating the 12 month average of each year centered on winter, i.e. July 1979 – June 1980, July 1980 – June 1981, etc. (b) uses only winter months October through March, and (c) uses only spring and summer months March through August, to create yearly records highlighting a particular season. (a) also shows the direction and relative speed in arrow size of 850 mb level winds from 5th July 2009 12:00 GMT (41), an example time period of a severe dust event in Tehran, Iran in which dust was sourced from the Mesopotamia region (25, 28). The location of paleoclimate records discussed in the text are marked with circles, labels provided in the legend in (a). Source area of 92% of contributions of PM_{10} (fine dust with particles smaller than $10\ \mu\text{m}$) in Tehran (50 km from label #9, *this study*) during 2009-2010 dusty episodes shown by dotted boxed area in (a) (28).

of an abrupt signal in this proxy may be expected, as speleothem $\delta^{18}\text{O}$ is complex and responds to climate change on a large spatial scale (eg. 18).

Drysdale et al. (2006) discovered a pronounced signal in other speleothem proxies (Mg/Ca, $\delta^{13}\text{C}$, and fluorescence measurements) at ≈ 4.2 ka (Fig. 2b) in a central Mediterranean flowstone sample from Buca della Ranella cave (Fig. 1, Label 3). Later higher resolution $\delta^{18}\text{O}$ work on the same sample (19) also indicated a $\delta^{18}\text{O}$ signal at this time and combined with other central Mediterranean records suggested that the event in this region was likely characterized by longer summer drought (19). Unfortunately, the age uncertainty on this particular flowstone is not an improvement over the marine records, so the timing and duration of the signal remains uncertain. Modern climate records also suggest that the central Mediterranean has little correlation with rainfall in northern Mesopotamia on inter-annual timescales, so the relevance of this site to the key archeological region is unclear (Fig. 1).

In this study, we aim to assess whether an unusual climate event is indeed evident at, or close to, the location of the north Mesopotamia settlements that show a large transition at this time. We investigate the magnitude and duration of climate variation in a precisely-dated mid-to-late Holocene record, and assess the uniqueness of the 4.2 ka event.

The Middle East is characterized by aridity, and the alluvial plains of the Tigris and Euphrates rivers are one of the major world source areas of dust (20). Dust storm activity is a function of climate in the source region, and can increase due to multiple inter-related factors (precipitation amount, vegetation cover, windspeed) (21), with sometimes large magnitude changes on abrupt timescales (22, 23). Cullen et al. (2000) captured an abrupt, factor-of-5 increase in eolian deposits from Mesopotamia at $4.1 \pm 0.1(1\sigma)$ ka in a Gulf of Oman marine sediment record (Fig. 2a). It is plausible that this dust event is captured in terrestrial archives, such as speleothems that can be sampled for trace elements at high resolution, if the concentration of particular

elements leached from the dust deposit is large compared with the karst limestone background concentrations.

Here we present an annual-to-decadal scale stalagmite multi-proxy record from northwest Iran spanning 5.2-3.7 ka. The record is dated at high resolution and contains large abrupt changes in Mg/Ca, which are explained by sensitivity to dust input to the overlying soil. An apparent threshold behavior between dustiness and aridity allows detailed assessment of change during the mid-Holocene, as well as a precise chronology for the 4.2 ka climatic event notably at a terrestrial site near to North Mesopotamia, the key region of societal change at this time.

New 4.2 ka record with precise age model

1. Cave from the Iranian plateau

The Iranian plateau is located directly to the east (downwind) of Mesopotamia. Rainfall patterns in west Iran (Zagros mountains) and north Iran (Alborz mountains) are correlated with Mesopotamia on seasonal to inter-annual timescales (Fig. 1), dominated by winter precipitation (SI Appendix). Gol-e-Zard ("Yellow Flower") cave (Fig. 1, Label 9) is situated on the southern slopes of the Alborz mountains (35.84°N , 52.00°E), 2535 meters above sea level (SI Appendix, Fig. S2). Stalagmite GZ14-1 was collected near the end of the cave's single $\approx 300\text{m}$ long passage in 2014 (SI Appendix).

Dust storms in the region, sourced from the Tigris-Euphrates alluvial plain in Syria and Iraq (24), are categorized into two groups: the summer Shamal, with highest event frequency in June and July, and frontal dust storms, the most common events in the non-summer season (25). The summer Shamal winds, strong north-westerlies near the surface, transport dust across Iraq, Kuwait, the Persian Gulf, and parts of the Arabian Peninsula (e.g. 26, 27). Givhechi et al. (2013) analyzed the 2009-2010 dusty episodes in Tehran, 50 km SW of Gol-e-Zard cave (*this study*) (SI Appendix, Fig. S2), and concluded that $\approx 90\%$ of the dust-related PM_{10} concentrations was sourced from the deserts of Syria and Iraq (SI Appendix, Fig. S3). Indeed, analysis of natural hazard-level Shamal dust storms between 2003-2011 show the two most common synoptic types associated with these dust storms to be capable of transporting dust to west and central Iran (Fig. 1 shows

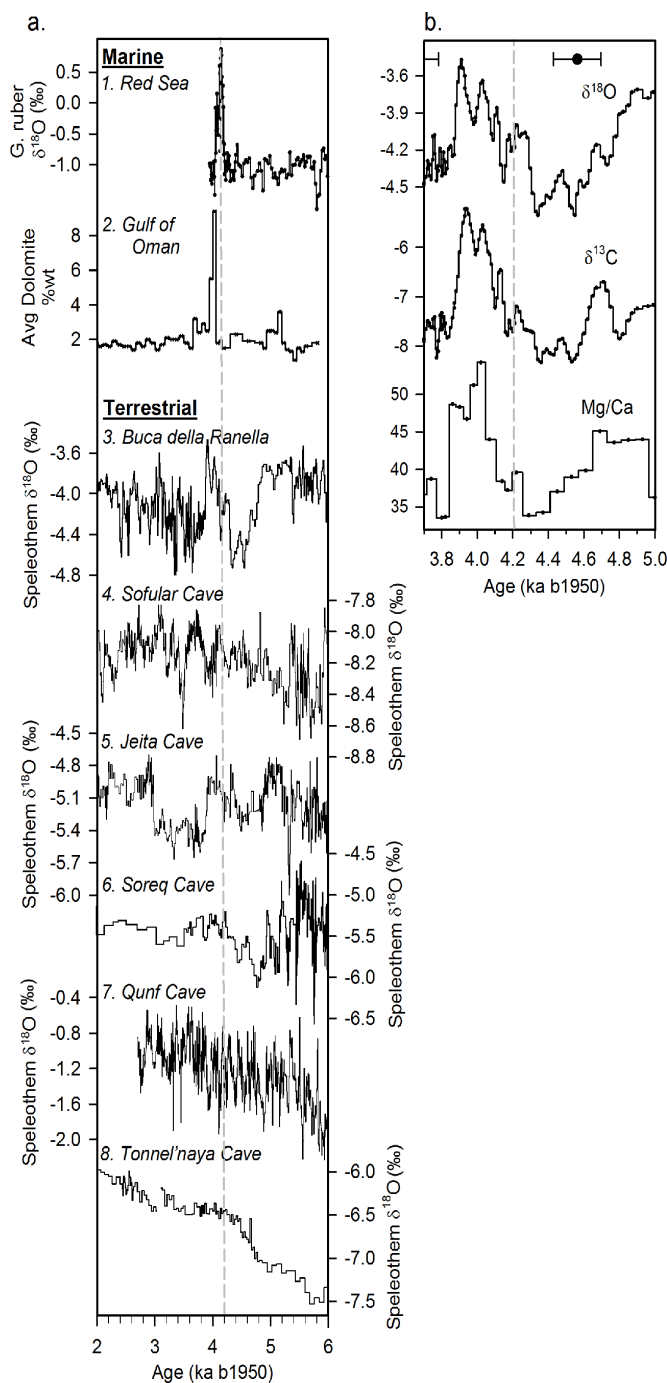


Fig. 2. . Mid-to-late Holocene records of climatology in the Mesopotamia region. (a) Marine records: (i) Red Sea sediment core GeoB 5836-2 shallow dwelling foraminifera *G. ruber* $\delta^{18}\text{O}$ (‰) (5) (ii) Gulf of Oman Core M5-422 eolian dolomite concentration (% wt) (3), and Terrestrial records: (iii) Buca della Ranella RL4 stalagmite $\delta^{18}\text{O}$ record (6, 19) (iv) Sofular cave So-1 stalagmite $\delta^{18}\text{O}$ record (42); (v) Jeita J-1 stalagmite $\delta^{18}\text{O}$ record (43); (vi) Soreq cave multiple stalactite and stalagmite $\delta^{18}\text{O}$ records (8, 44); (vii) Qunf cave Q5 stalagmite $\delta^{18}\text{O}$ record (45); (viii) Tonnel'naya cave TON-2 stalagmite $\delta^{18}\text{O}$ record (46). Locations of the caves are shown in Fig. 1. (b) Local climate proxies, Mg/Ca (mmol/mol) and $\delta^{13}\text{C}$ (‰), measured in the Buca della Ranella RL4 stalagmite (6, 19) are plotted with the new high-resolution $\delta^{18}\text{O}$ (‰) record (19), all on the updated age model (19). A grey dotted line in both (a) and (b) indicates the location of date 4.2 ka before 1950 C.E.

the 850mb winds of a destructive dust storm observed in Iran in July 2009) (25, 28). Additionally, analysis of frontal dust storms

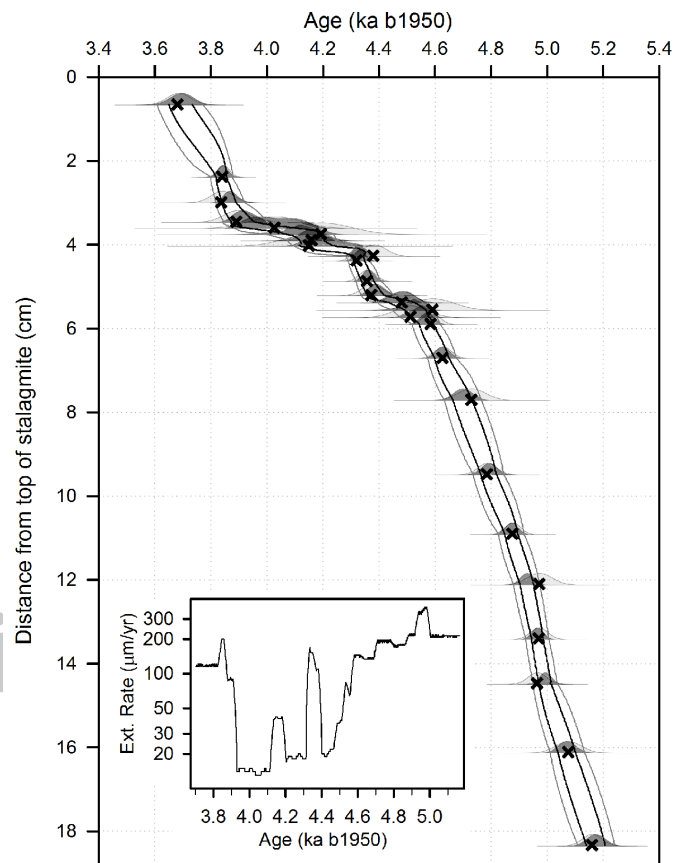


Fig. 3. . GZ14-1 age v. depth plot with OxCal Poisson process deposition age model 68% (black) and 95% (dark grey) confidence ranges (30, 31). Original individual U-series samples' ages are plotted as black "x" shapes. Individual samples' modeled age distributions are shown in dark grey (68%) and light grey (95%). GZ14-1's mean extension rate ($\mu\text{m/yr}$), plotted as a 20-yr moving average of the annually interpolated OxCal mean extension rate, is included as a subset in the lower left corner.

show a synoptic pattern that transports dust north-eastwards to west and central Iran, and in extreme cases as far north as the Caspian coast (25). As rainfall occurs almost exclusively during the winter months in the Middle East region, there is minimal precipitation along the dust transport path during the summer Shamal. Gravitational settling is thus the dominant mechanism for atmospheric scavenging (21).

Gol-e-Zard cave receives an average ≈ 380 mm precipitation annually, with ≈ 50 mm total accumulated rainfall in June-September, 10-times greater than the surrounding plateau, due to its higher elevation (29) (*SI Appendix, Fig. S4*). Typical monthly surface temperatures above the cave range from -12°C in the winter to 26°C in the summer, and the site is covered with snow in the winter (29) (*SI Appendix, Fig. S5 and S6*). The temperature within the cave is assumed to be the average annual temperature, $\approx 7^\circ\text{C}$.

II. Timing of arid periods

Twenty-five U/Th dates (*Methods; SI Appendix, Fig. S7 and S8, Table S3*) and thin section analysis indicate that stalagmite GZ14-1 grew with no recognizable hiatuses from 5.2 to 3.7 ka, covering the age of the decline of the Akkadian empire and abandonment of urban settlements in northern Mesopotamia. The age model, with 68% and 95% confidence ranges, was constructed using OxCal's Poisson-process deposition model (30, 31) and has an average age error of 31 years (1σ) (*Methods, SI Appendix*), with larger errors during the slower growth periods (**Fig. 3; SI Appendix, Dataset S1**). GZ14-1 grew relatively quickly throughout

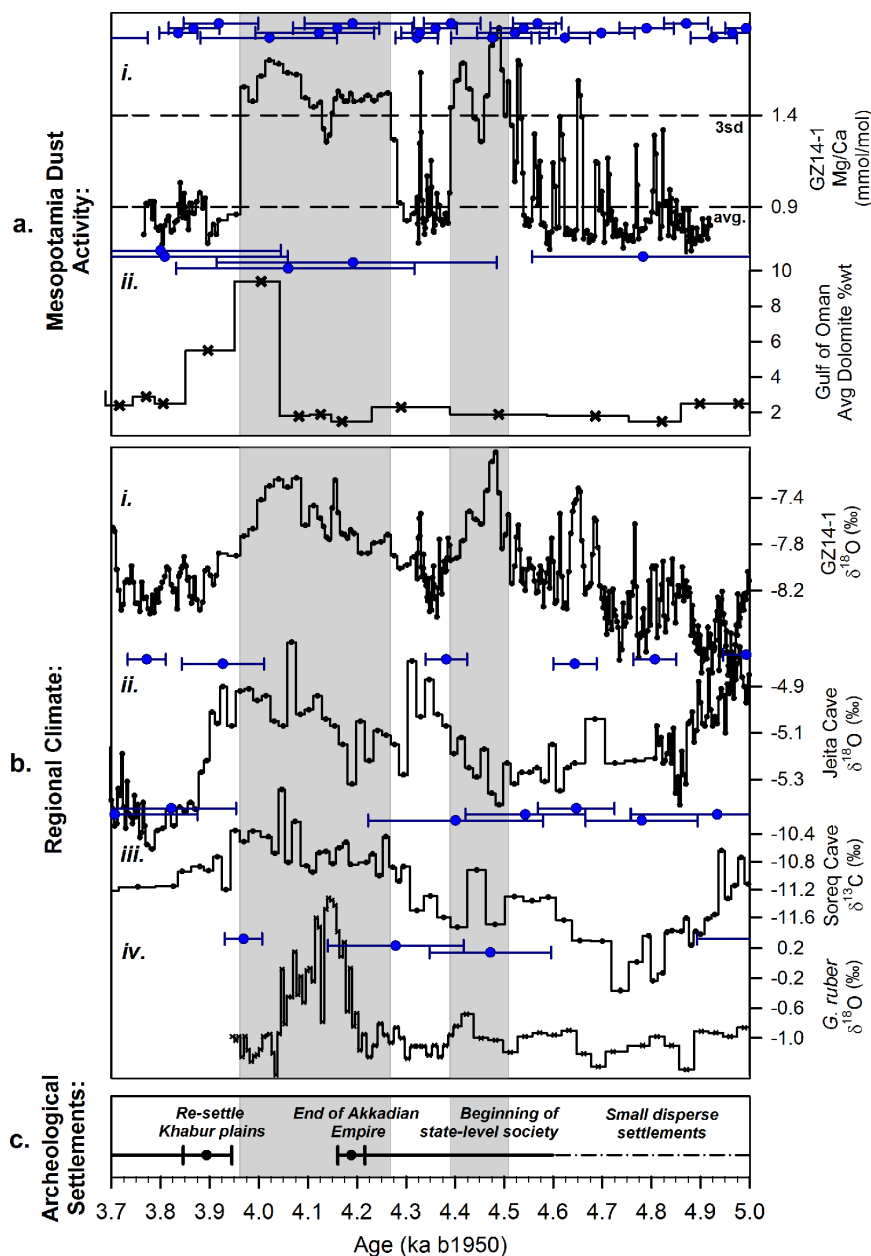


Fig. 4. Timing of environmental changes in Middle East region compared with archeological settlement records. (a) Proxy records of Mesopotamia-sourced dust event activity: (i) GZ14-1 Mg/Ca (mmol/mol) (*this study*) and (ii) Gulf of Oman Core M5-422 eolian dolomite concentration (% wt) (3), plotted on an updated age model (*SI Appendix*). Time resolution of GZ14-1 is average of ~ 2 years during fast growth and average of ~ 10 -15 years during slow growth, with slow growth period found within intervals highlighted in grey (growth rate shown in Fig. 3). In both records greater Mg/Ca or dolomite % wt indicates more dolomite-containing eolian dust deposits. (b) Proxy records of aridity climate: (i) GZ14-1 $\delta^{18}\text{O}$ (*this study*), with more positive values interpreted as drier conditions to an unknown magnitude on inter-annual timescales, (ii) Jeita cave stalagmite $\delta^{18}\text{O}$ record as in Fig 2a; more enriched $\delta^{18}\text{O}$ interpreted as drier conditions (43), (iii) Soreq cave multiple stalactite and stalagmite sample $\delta^{13}\text{C}$ records; more enriched $\delta^{13}\text{C}$ interpreted as drier conditions (8, 44), (iv) Red Sea sediment core GeoB 5836-2 *G. ruber* $\delta^{18}\text{O}$, as in Fig. 2a; more enriched $\delta^{18}\text{O}$ interpreted as greater evaporation and thus drier climate (5). (c) Graphical representation of the evolution of rain-fed agricultural settlements in north Mesopotamia, which became urbanized around 4.5 ka, were imperialized by Akkad around 4.26 ka, and then were suddenly abandoned at $4.19 \pm 0.018(1\sigma)$ ka (17), coincident with the decline of the Akkadian empire. Settlements returned at $3.90 \pm 0.026(1\sigma)$ ka (17). Modeled U/Th mean ages (blue circles) and 95% confidence ranges are plotted above each record. For the two GZ14-1 records, (a)(i) and (b)(i), the ages are plotted only above (a)(i). The two vertical grey bars across all panels begin when Mg/Ca ratio in the GZ14-1 record rises greater than 3σ from the average ratio of the record for >10 years, and end when Mg/Ca returns to background levels (see *Methods, Event timing and errors*).

the majority of the record ($>130 \mu\text{m/yr}$). However, in two periods the extension rate, or vertical growth rate, falls below $100 \mu\text{m/yr}$, dropping to ≈ 15 - $20 \mu\text{m/yr}$: 4.57-4.38 ka and 4.32-3.91 ka (start-to-end date) (Fig. 3). The decreased extension rate is suggestive of drier local conditions, however it is important to note that other factors not directly related to rainfall, such as drip rate, temperature, and dripwater chemistry, also are capable of affecting the extension rate (e.g. 32). Thus without complementary proxies the extension rate in a single stalagmite is inconclusive.

The ratio of Mg/Ca in GZ14-1 exhibits sudden changes coincident with the periods of slow vertical growth. Mg/Ca abruptly increases at the start of two periods, lasting from 4.51 to 4.40 ka and from 4.26 to 3.97 ka (Fig. 4a) (*Methods*). Error in the start and end dates of these periods range between 40-70 years (1σ) due to the slow growth rate of this interval (*SI Appendix, Dataset S1*).

The rise in GZ14-1 Mg/Ca is most readily interpreted as an increase in Mesopotamia-sourced dust. Mineralogical studies show that dust sourced from this region contains dolomite (33, 34), and a greater dust flux and deposition over the Gol-e-Zard cave site is likely to result in a greater Mg/Ca ratio in dripwaters through dissolution of the dust particulates in the soil above the cave (*SI Appendix*). Occasional rainfall in the summer months and snow cover in the winter months may also help prevent the dust from being blown off before dissolution.

Increased prior calcite precipitate (PCP), a term used to describe the precipitation of calcite within the karst conduits before the dripwater arrives on the stalagmite, is a second mechanism that could increase stalagmite Mg/Ca ratios (35). This mechanism can be ruled out as the major cause of Mg/Ca change in this record, however, because other element and isotopic ratios affected by PCP, such as Sr/Ca, Ba/Ca, and $\delta^{13}\text{C}$, do not follow the expected behavior associated with PCP (*SI Appendix, Fig. S10*).

A mass balance calculation based on the concentration of trace elements in the host rock that allows for dissolution of dolomite-containing dust can produce the observed magnitude shift in Mg/Ca, Sr/Ca, and Ba/Ca ratios, supporting such dust dissolution as the major control on Mg/Ca (*SI Appendix, Fig. S11*).

Discussion

This study shows two centennial-scale periods of high Mg/Ca with abrupt beginnings and ends (**Fig. 4a**). The events demonstrate threshold behavior in dustiness of the Mesopotamia region, due to either enhanced aridity, stronger winds, or change in soil properties or vegetation cover (21). Several factors suggest a drier regional climate coincident with these two century-scale dusty periods. The stalagmite was collected from a site at which inter-annual rainfall variability today is positively correlated with rainfall variability in north Mesopotamia (**Fig. 1**, Label 9). During the two periods of anomalously high Mg/Ca, the stalagmite $\delta^{18}\text{O}$ record exhibits a gradual increase followed by a decrease back to baseline values (**Fig. 4b**). Based on the limited modern rainfall $\delta^{18}\text{O}$ data available, the increased stalagmite $\delta^{18}\text{O}$ can be interpreted as a decrease in precipitation amount at Gol-e-Zard cave: rainwater $\delta^{18}\text{O}$ at Tehran (50 km SW of the cave site) between 1962–1972 (36) has a negative correlation with annual average precipitation amount (51% of the variance in $\delta^{18}\text{O}_{\text{rainwater}}$ is predictable from rainfall amount) (*SI Appendix, Fig. S13*). The stalagmite multi-proxy record is therefore interpreted as two periods when enhanced dustiness was caused by some threshold behavior, in which the region became sufficiently dry that dust sources increased dramatically. Similar behavior has been seen in other settings, notably during variation in aridity in North Africa (22, 23).

Additional information on regional climate during the dusty periods is found in other nearby speleothem records, which show stable isotope enrichment, interpreted as evidence of more arid conditions, around the same periods as the Iranian stalagmite Mg/Ca dust-proxy events (**Fig. 4b**). The records support our interpretation of drying in the region during these two periods. However, the stable isotope proxies in other speleothem records are not exhibiting abrupt or anomalous shifts and therefore do not allow for as precise a chronology of climate variations as is obtained using the Iranian Mg/Ca proxy (**Fig. 4**).

The Red Sea sediment record (**Fig. 1**, Label 1) does show a clear, anomalous +2‰ increase in planktonic $\delta^{18}\text{O}$, interpreted as drier conditions and enhanced evaporation in the region, from 4.2 to 4.0 (± 0.1 ; 1 σ) ka, with perhaps an earlier period of less extreme aridity (indicated by a +0.3‰ $\delta^{18}\text{O}$ increase) from 4.5 to 4.4 (± 0.1 ; 1 σ) (**Fig. 4b**) (5). The Gulf of Oman record (3) only demonstrates one period of dustiness (at 4.1 ± 0.1 , 1 σ ka), and no earlier event at ≈ 4.5 ka (**Fig. 4a**). Taken with the new results from this study, these records demonstrate the presence of two arid periods, but indicate that the later of these – at 4.2 ka – is of larger amplitude and has a greater spatial extent, apparently influencing the broad Middle Eastern region. The precise chronology of the record presented here allows the duration of these two events to be assessed, and demonstrates the event starting at 4.2 ka was of longer duration, as well as larger extent, than the earlier 4.5 ka event (≈ 290 versus ≈ 110 years).

A hierarchy of urbanized settlements and structured economies in northern Mesopotamia (e.g. 13) were abandoned at 4.19 ± 0.02 (1 σ) (**Fig. 4c**) (17). These abandoned settlements, which are connected with the wider decline of the Akkadian Empire, do not show evidence of repopulation until 3.90 ± 0.03 (1 σ), ≈ 300 years later (17). The Iran stalagmite climate proxy record is strategically located in close proximity to the settlements, to challenge the originally proposed linkage (12) between human societal transformations in north Mesopotamia and climate change. The Mg/Ca record suggests an abrupt start

and end to a ≈ 300 year dusty period at this time (**Fig. 4a**), overlying a more gradual trend toward maximum aridity seen in the $\delta^{18}\text{O}$ record. A two-tailed student t-test (*SI Appendix*) confirms the statistical significance of indistinguishable ages between the onset of abrupt dust event (4.26 ± 0.066 (1 σ) ka) and the timing of settlement collapse in north Mesopotamia (4.19 ± 0.017 (1 σ) ka), supporting the possibility of a relation between the two. Further, the remarkably similar duration of the dusty/arid event (≈ 290 years) with the duration of the abandoned settlements (≈ 300 years) provides additional support for a relationship between the two. It is possible that the link is explained by the fact that these agricultural settlements were located in marginal areas particularly vulnerable to variations of aridity.

The Iran stalagmite record of this study delivers a significantly improved age model that for the first time is able to capture the precise start and end points for two periods of “switched on” dust events originating in Mesopotamia, as well as the duration of these periods, between 5.2–3.7 ka. The second period of heightened dust flux, suggested to be of greater magnitude and/or larger regional extent, occurs within decadal-scale error of the decline of the Akkadian empire and abandonment of advanced urban settlements in north Mesopotamia (4.19 ± 0.02 (1 σ) ka), strengthening the case for association between societal and environmental change. Comparison with the sample’s stable isotope record and regional speleothem and marine paleoclimate records support the idea that both periods of switched on dust activity coincide with periods of drier climate, and that the later 290-year period beginning at 4.26 ± 0.066 (1 σ) ka was more extreme in magnitude than the earlier shorter period. Evidence of centennial-scale periods of enhanced dust activity in the Middle East that begin abruptly and correspond with a slower trend toward drier conditions in the region provides additional insight on the magnitude of natural climate variability in this region, notably within global climate parameters that are similar to present.

Methods:

U/Th ages: Stalagmite GZ14-1 was sliced in half vertically using a tile saw, and 80–230 mg calcite samples (weight varying due to size of lamina and distance from other U/Th ages) were drilled with a 0.8mm or 1.0mm diameter drill bit at various distances from the top of the stalagmite (*SI Appendix, Fig. S7*). Sample drill depth into the stalagmite half was ≈ 2 –3mm. The powder calcite samples were dissolved in nitric acid and spiked with a mixed ^{229}Th – ^{236}U solution (37) and the U and Th fractions were separated following procedures adapted from Edwards et al. (1986). U and Th isotopes were measured using a Nu Plasma multi-collector inductively coupled plasma mass spectrometer (MC-ICP-MS) at Oxford University, following the procedures described in Vaks et al. (2013). Individual ages and 95% confidence intervals were calculated using an in-house Monte Carlo script that incorporates chemical blank errors, analytical uncertainties, and the initial $^{230}\text{Th}/^{232}\text{Th}$ ratio of 5.38 ± 5.38 ppm (uniform distribution) (*SI Appendix, Table S3*).

Age model: The age model with 68% and 95% confidence ranges was produced using OxCal Version 4.3 Poisson-process deposition model ($k_0 = 1 \text{ cm}^{-1}$, $\log_{10}(k/k_0) = U(-2,2)$), with interpolation (30, 31) (*SI Appendix, Table S4 and Dataset S1*).

Proxy sample extraction: The working half of GZ14-1 was slabbed and mounted to a New Wave MicroMill. Element and stable isotope powder samples were drilled with a flat-base, cylindrical 0.8mm diameter tungsten-carbide drill bit in a trench along the growth axis at 500 μm and 250 μm step intervals for initial low resolution sampling, followed by 100 μm and 50 μm step intervals for high-resolution sampling. Depth of drilling was ≈ 500 μm for low resolution and ≈ 1000 μm for high resolution, and the width perpendicular to growth axis was 2.5mm for the high-resolution samples (*SI Appendix, Fig. S7*). ≈ 500 –1000 μg powders were collected individually using aluminum spatulas and stored in compressed air-cleaned plastic 2ml centrifuge tubes.

Trace element/Ca ratios: 80–100 μg of calcite was removed from the storage tubes using an ethanol-cleaned spatula and analyzed for a suite of trace elements (Mg, Sr, Ba, S, Na, K, P, Cr, Mn, Fe, Co, Zn, U) using a Thermo Scientific Element 2 ICP-MS at Oxford University. All samples (calcite and water samples) were diluted to 10 ppm Ca concentration for analysis. Calibration standards bracketed every 20 samples to correct for drift, and a secondary standard was measured every 10 samples to calculate precision/accuracy. Trace element-to-Ca ratios were determined using the

'ratio' method (40). Mg/Ca, Sr/Ca, Ba/Ca, and S/Ca records provided in *SI Appendix, Dataset S2*.

Stable isotope ratios: 30–60 µg of calcite was removed from the storage tubes using an ethanol-cleaned spatula and analyzed for oxygen and carbon stable isotopes using a Thermo Scientific Delta V isotope ratio mass spectrometer (IRMS) coupled to a Kiel V carbonate device at Oxford University. Each batch (up to 38 samples) was measured with calibration standards and evenly scattered secondary standards. Precision/accuracy was calculated using the secondary standards' long-term average and standard deviation ($\delta^{18}\text{O} = \pm 0.07\text{‰}$, $\delta^{13}\text{C} = \pm 0.05\text{‰}$, 1 σ). $\delta^{18}\text{O}$ and $\delta^{13}\text{C}$ records provided in *SI Appendix, Dataset S2*. Water sample hydrogen and oxygen stable isotopes were measured on the same Delta V IRMS using a Thermo Scientific Gasbench II gas preparation and introduction system. Water calibration standards and evenly scattered secondary standards were used for water analyses ($\delta^{18}\text{O} = \pm 0.09\text{‰}$, 1 σ).

XRD analysis: $\approx 0.2\text{--}5$ mg powder samples (smaller samples for GZ14-1, larger samples for overlying rock) were analyzed using a PANalytical Empyrean Series 2 powder diffractometer at Oxford University. HighScore software was used to detect peaks and measure peak size, and calculate percentage of mineral in the sample based on user-chosen mineral candidates. Candidates were chosen based on i) if the most intense peaks for that mineral occurred in the data, and ii) if the mineral assemblage makes sense given prior knowledge of the sample.

Event timing and errors: Linear interpolation was used to create a 10yr-resolution Mg/Ca record (*SI Appendix, Dataset S3*). A histogram of the Mg/Ca ratios was then plotted, which shows a bimodal distribution, with

the lower-value peak indicating background values and the higher-value peak indicating event-linked values (*SI Appendix, Fig. S14*). 1.4 mmol/mol was chosen as the maximum cutoff for background values based on the location of peaks in the bimodal distribution, and values greater than 1.4 mmol/mol were removed to calculate the average and standard deviation of the record (0.87 ± 0.18 (1 σ) mmol/mol). Post-calculation, 1.4 mmol/mol is equal to adjusted average + 3 σ . The age and age error associated with the depth at which the Mg/Ca ratio rises above/below 1.4 mmol/mol for longer than 10 years ("event") was obtained from the interpolated OxCal age model.

Acknowledgements:

We sincerely thank Vahid Ashrafi, Saeed Hasheminezhad and Javad Nezamdoost from the Iranian Cave and Speleology Association who were instrumental in fieldwork and sample collection. We thank S. Hemming and the participants of the Comer Changelings Conference, as well as D. Fleitmann, S.L. Jones, G. Zanchetta, H. Weiss, M. Wencel, and the RLAHA lab group at Oxford University for helpful discussions in preparation of the manuscript. We thank Oxford undergraduate student Luke Maxfield for his assistance in milling and analyzing stable isotope and trace element samples. We thank A. Hsieh for his assistance with the MC-ICP-MS, and P. Holdship for his assistance with the Element ICP-MS. We also thank H. Sodemann for his assistance in producing back trajectory plots to track the source of rainwater in the Tehran region. We are grateful for the editorial handling of our manuscript and helpful anonymous reviewer input. This research was supported by the Leverhulme Trust, Research Project Grant RPG-2013-235.

- Höflmayer, F (2017) The late third millennium B.C. in the ancient near east and eastern Mediterranean: a time of collapse and transformation. In F Höflmayer ed. *The late third millennium in the ancient Near East: Chronology, C14, and climate change* (The University of Chicago, Chicago).
- Gasse F, Van Campo E (1994) Abrupt post-glacial climate events in West Asia and North Africa monsoon domains. *Earth and Planetary Science Letters* 126(4):435–456.
- Cullen HM, et al. (2000) Climate change and the collapse of the Akkadian empire: Evidence from the deep sea. *Geology* 28(4):379.
- Thompson LG (2002) Kilimanjaro Ice Core Records: Evidence of Holocene Climate Change in Tropical Africa. *Science* 298(5593):589–593.
- Arz HW, Lamy F, Pätzold J (2006) A Pronounced Dry Event Recorded Around 4.2 ka in Brine Sediments from the Northern Red Sea. *Quaternary Research* 66(03):432–441.
- Drysdale R, et al. (2006) Late Holocene drought responsible for the collapse of Old World civilizations is recorded in an Italian cave flowstone. *Geology* 34(2):101.
- Parker AG, et al. (2006) A Record of Holocene Climate Change from Lake Geochemical Analyses in Southeastern Arabia. *Quaternary Research* 66(03):465–476.
- Bar-Matthews M, Ayalon A (2011) Mid-Holocene climate variations revealed by high-resolution speleothem records from Soreq Cave, Israel and their correlation with cultural changes. *The Holocene* 21(1):163–171.
- Geirsdóttir Á, Miller GH, Larsen DJ, Ólafsdóttir S (2013) Abrupt Holocene climate transitions in the northern North Atlantic region recorded by synchronized lacustrine records in Iceland. *Quaternary Science Reviews* 70:48–62.
- Salzer MW, Bunn AG, Graham NE, Hughes MK (2014) Five millennia of paleotemperature from tree-rings in the Great Basin, USA. *Climate Dynamics* 42(5–6):1517–1526.
- van der Bilt WGM, et al. (2015) Reconstruction of glacier variability from lake sediments reveals dynamic Holocene climate in Svalbard. *Quaternary Science Reviews* 126:201–218.
- Weiss H, et al. (1993) The Genesis and Collapse of Third Millennium North Mesopotamian Civilization. *Science* 261(5124):995–1004.
- Weiss H (2017) Seventeen Kings Who Lived in Tents. In F Höflmayer ed. *The late third millennium in the ancient Near East: Chronology, C14, and climate change* (The University of Chicago, Chicago).
- Monnin E, et al. (2004) Evidence for substantial accumulation rate variability in Antarctica during the Holocene, through synchronization of CO₂ in the Taylor Dome, Dome C and DML ice cores. *Earth and Planetary Science Letters* 224(1–2):45–54.
- Global Volcanism Program, 2013. Volcanoes of the World, v. 4.6.6. Venzke, E (ed.). Smithsonian Institution. Downloaded 04 Mar 2018. <https://dx.doi.org/10.5479/si.GVPVOTW4-201>.
- Steinhilber F, et al. (2012) 9,400 years of cosmic radiation and solar activity from ice cores and tree rings. *Proceedings of the National Academy of Sciences* 109(16):5967–5971.
- Weiss et al. (2012) Tell Leilan Akkadian imperialism, collapse, and short-lived reoccupation defined by high-resolution radiocarbon dating. In Weiss H ed. *Seven generations since the fall of Akkad* (Harrassowitz Verlag, Wiesbaden).
- McDermott F, Atkinson TC, Fairchild IJ, Baldini LM, Matthey DP (2011) A first evaluation of the spatial gradients in $\delta^{18}\text{O}$ recorded by European Holocene speleothems. *Global and Planetary Change* 79(3–4):275–287.
- Zanchetta G, et al. (2016) The so-called "4.2 event" in the central mediterranean and its climatic teleconnections. *Alpine and Mediterranean Quaternary*, 29(1):5–17.
- Grigoryev, AA, Kondratyev, KJ (1980) Atmospheric dust observed from space. Part 1: Analysis of pictures. *WMO Bulletin*, 29: 250–255.
- Clemens SC (1998) Dust response to seasonal atmospheric forcing: Proxy evaluation and calibration. *Paleoceanography* 13(5):471–490.
- deMenocal P, et al. (2000) Abrupt onset and termination of the African Humid Period: *Quaternary Science Reviews* 19(1–5):347–361.
- McGee D, deMenocal PB, Winkler G, Stuut JWB, Bradtmiller LI (2013) The magnitude, timing and abruptness of changes in North African dust deposition over the last 20,000yr. *Earth and Planetary Science Letters* 371–372:163–176.
- Cao H, Amiraslani F, Liu J, Zhou N (2015) Identification of dust storm source areas in West Asia using multiple environmental datasets. *Science of The Total Environment* 502:224–235.
- Hamidi M, Kavianpour MR, Shao Y (2013) Synoptic analysis of dust storms in the Middle East. *Asia-Pacific Journal of Atmospheric Sciences* 49(3):279–286.
- Middleton, NJ (1986). *The geography of dust storms* (Doctoral Thesis). Retrieved from <https://ora.ox.ac.uk/objects/uuid:9e98cc16-7a43-4ef8-9526-3e4c064b108a>. (Source Identifier 602354639).
- Yu Y, Notaro M, Kalashnikova OV, Garay MJ (2016) Climatology of summer Shamal wind in the Middle East: Summer Shamal Climatology. *Journal of Geophysical Research: Atmospheres* 121(1):289–305.
- Givhechi R, Arhami M, Tajrishy M (2013) Contribution of the Middle Eastern dust source areas to PM10 levels in urban receptors: Case study of Tehran, Iran. *Atmospheric Environment* 75:287–295.
- European Centre for Medium-Range Weather Forecasts. 2017, updated monthly. ERA5 Reanalysis. Research Data Archive at the NCAR CISL. <https://doi.org/10.5065/D6X34W69>. Accessed 15 Jan 2017. *Generated using Copernicus Climate Change Service Information. Neither the European Commission nor ECMWF is responsible for any use that may be made of the information it contains.*
- Bronk Ramsey C (2008) Deposition models for chronological records. *Quaternary Science Reviews* 27(1–2):42–60.
- Bronk Ramsey C, Lee S, (2013) Recent and Planned Developments of the Program OxCal. *Radiocarbon*, 55(2–3), 720–730.
- Day CC, Henderson GM (2011) Oxygen isotopes in calcite grown under cave-analogue conditions. *Geochimica et Cosmochimica Acta* 75(14):3956–3972.
- Hojati S, Khademi H, Faz Cano A, Landi A (2012) Characteristics of dust deposited along a transect between central Iran and the Zagros Mountains. *CATENA* 88(1):27–36.
- Ahmady-Birgani H, Mirnejad H, Feiznia S, McQueen KG (2015) Mineralogy and geochemistry of atmospheric particulates in western Iran. *Atmospheric Environment* 119:262–272.
- Fairchild IJ, et al. (2000) Controls on trace element (Sr–Mg) compositions of carbonate cave waters: implications for speleothem climatic records. *Chemical Geology* 166(3–4):255–269.
- AEA/WMO (2018). Global Network of Isotopes in Precipitation. The GNIP Database. Accessible at: <http://www.iaea.org/water>
- Robinson LF, Belshaw NS, Henderson GM (2004) U and Th concentrations and isotope ratios in modern carbonates and waters from the Bahamas. *Geochimica et Cosmochimica Acta* 68(8):1777–1789.
- Lawrence Edwards R, Chen JH, Wasserburg GJ (1987) 238U–234U–230Th–232Th systematics and the precise measurement of time over the past 500,000 years. *Earth and Planetary Science Letters* 81(2–3):175–192.
- Vaks A, et al. (2013) Speleothems Reveal 500,000-Year History of Siberian Permafrost. *Science* 340(6129):183–186.
- Rosenthal Y, Field MP, Sherrell RM (1999) Precise Determination of Element/Calcium Ratios in Calcareous Samples Using Sector Field Inductively Coupled Plasma Mass Spectrometry. *Analytical Chemistry* 71(15):3248–3253.
- Dee DP, et al. (2011) The ERA-Interim reanalysis: configuration and performance of the data assimilation system. *Quarterly Journal of the Royal Meteorological Society* 137(656):553–597. *Generated using Copernicus Climate Change Service Information. Neither the European Commission nor ECMWF is responsible for any use that may be made of the information it contains.*
- Fleitmann D, et al. (2009) Timing and climatic impact of Greenland interstadials recorded in stalagmites from northern Turkey. *Geophysical Research Letters* 36(19).
- Cheng H, et al. (2015) The climate variability in northern Levant over the past 20,000 years. *Geophysical Research Letters* 42(20):8641–8650.
- Grant KM, et al. (2012) Rapid coupling between ice volume and polar temperature over the past 150,000 years. *Nature* 491:744–747.
- Fleitmann D, et al. (2007) Holocene ITCZ and Indian monsoon dynamics recorded in stalagmites from Oman and Yemen (Socotra). *Quaternary Science Reviews* 26(1–2):170–188.
- Cheng H, et al. (2016) Climate variations of Central Asia on orbital to millennial timescales. *Scientific Reports* 5:36975.

817
818
819
820
821
822
823
824
825
826
827
828
829
830
831
832
833
834
835
836
837
838
839
840
841
842
843
844
845
846
847
848
849
850
851
852
853
854
855
856
857
858
859
860
861
862
863
864
865
866
867
868
869
870
871
872
873
874
875
876
877
878
879
880
881
882
883
884

47.

885
886
887
888
889
890
891
892
893
894
895
896
897
898
899
900
901
902
903
904
905
906
907
908
909
910
911
912
913
914
915
916
917
918
919
920
921
922
923
924
925
926
927
928
929
930
931
932
933
934
935
936
937
938
939
940
941
942
943
944
945
946
947
948
949
950
951
952

Submission PDF